PERGAMON

Journal of Structural Geology 23 (2001) 279–296

JOURNAL OF STRUCTURAL GEOLOGY

www.elsevier.nl/locate/jstrugeo

Joint development during fluctuation of the regional stress field in southern Israel

Yehuda Eyal[a,*], Michael R. Gross[b], Terry Engelder[c], Alexander Becker[d]

[a]*Department of Geology and Environmental Sciences, Ben Gurion University, Beer Sheva 84105, Israel*
[b]*Department of Geology, Florida International University, Miami, FL 33199, USA*
[c]*Department of Geosciences, The Pennsylvania State University, University Park, PA 16802, USA*
[d]*Elayne Nominees Pty Ltd, 1061 Brickley Close, North Saanich, BC, Canada V8L 5L1*

Received 14 January 2000; accepted 6 June 2000

Abstract

Four trends of joint sets (WNW–ESE, NW–SE, NNW–SSE and NE–SW) are found in upper Turonian carbonate rocks within the Neqarot syncline of south-central Israel. The two most predominant sets strike parallel to the trend of maximum compressive stress directions (S_H) associated with the plate-related Syrian Arc stress field (SAS; WNW–ESE) active during the Cretaceous to present and the perturbed regional stress field (NNW–SSE) related to stress accumulation on the Dead Sea Transform during the Miocene to the present. Eighty-two percent of the beds in this study contain joints parallel with the latter trend, whereas 42% contain joints parallel to the former trend. All beds with layer thickness to spacing ratio (FSR) > 1.5 have NNW–SSE joint sets compatible with the Dead Sea Transform stress field (DSS), whereas all joints sets that are not compatible with the DSS stress field fall beneath this value for FSR. Considering lithology, joints in five of six chalky limestone beds and all marly limestone beds are compatible with the DSS, whereas joints compatible with the SAS do not develop in these marly and chalky limestone beds. In the study area, the joint sets lack a consistent formation sequence where more than one set is found in a single bed. We use these observations to conclude that all studied joints are Miocene or younger, that the regional stress field from the Miocene to the present fluctuated, between DSS and SAS states, and that the higher FSRs correspond to a greater amount of joint-normal strain in response to the DSS.

1. Introduction

1.1. Joints in layered rocks

Stratigraphic layering contributes to several unique characteristics of joint formation. Many joints in more competent lithologies terminate at bed boundaries. This effect often limits joint height to a mechanical unit of one or several stratigraphic beds, which define a mechanical layer thickness, MLT (e.g. Narr and Suppe, 1991; Gross et al. 1995). Joints in layered rocks often display a regular spacing, with joint spacing linearly proportional to mechanical layer thickness (e.g. Bogdonov, 1947; Price, 1966; Ladeira and Price, 1981; Narr and Suppe, 1991; Huang and Angelier, 1989; Gross, 1993; Engelder et al., 1997; Ji and Saruwatari, 1998). A suggested mechanism for this proportionality is the reduction in joint-normal tensile stress, or the increase in joint-normal compressive stress, in the immediate vicinity of a pre-existing joint, which inhibits the formation of new joints (Lachenbruch, 1961; Hobbs, 1967; Narr and Suppe, 1991; Gross, 1993; Fischer et al., 1995; Ji and Saruwatari, 1998; Bai and Pollard, 2000). The lateral extent of this zone of perturbed stress is proportional to joint height, which in turn is commonly equal to mechanical layer thickness.

Although the lateral extent of perturbed stress exerts a primary control on joint development, numerous exceptions to the layer thickness–joint spacing relationship are observed in layered rocks. This may result from the influence of other factors on joint development, such as lithology (Gross et al., 1995; Ji and Saruwatari, 1998), degree of joint set development (Rives et al., 1992; Wu and Pollard, 1995), magnitude of tectonic strain/proximity to faults and other structures (Becker and Gross, 1996; Gross et al., 1997), and interlayer slip (Ji et al., 1998). In light of the commonly observed proportionality of joint spacing to layer thickness, several workers have proposed that rock layers become "saturated" with joints and any additional joint-normal strain is accommodated by other types of deformation (e.g. bedding plane slip, opening of existing joints) rather than the formation of new joints

* Corresponding author. Tel.: 00-972-7-646-1332.
E-mail address: eyal@bgumail.edu.ac.il

0191-8141/01/$ - see front matter
PII: S0191-8141(00)00096-1

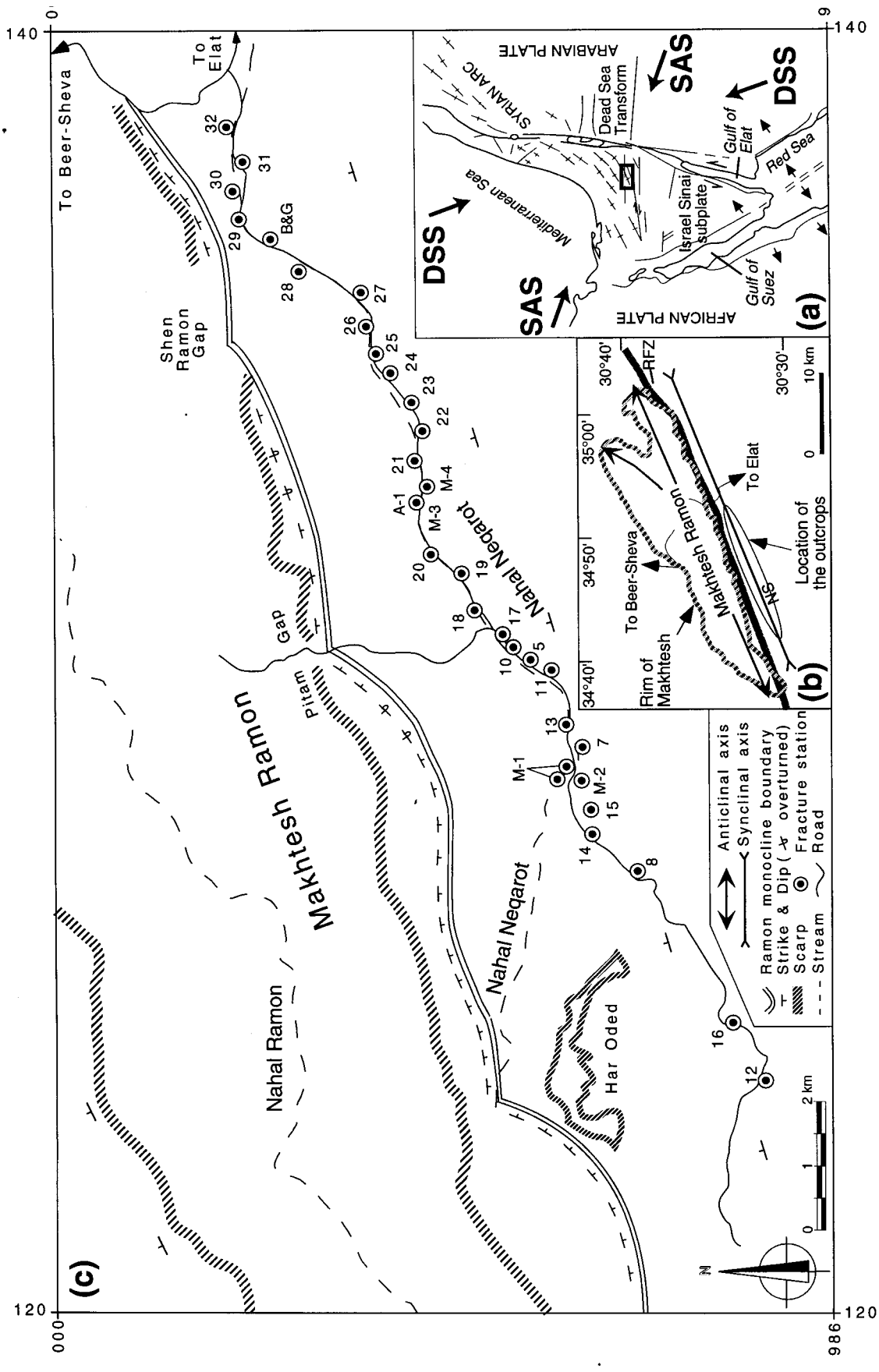

Fig. 1. (a) Generalized tectonic map of Israel and Sinai subplate showing location of study area and orientations of the maximum horizontal stress directions (S_H) for the Dead Sea stress field (DSS) and Syrian Arc stress field (SAS). (b) Location of outcrops with respect to the Ramon anticline (outlined by an erosional cirque known as Makhtesh Ramon), the Ramon fault zone (RFZ), and the Neqarot syncline (NS). (c) Location of fracture stations in the Gerofit Formation along the dry river bed of Nahal Neqarot and general structure of the southern flank of the Ramon anticline.

between the old ones (Narr and Suppe, 1991; Wu and Pollard, 1995; Renshaw, 1997). Proposed mechanisms for joint saturation include dramatically reduced tensile stresses between closely spaced joints (Lachenbruch, 1961; Hobbs, 1967) and the development of compressive stresses between adjacent joints (Bai and Pollard, 2000). The validity of saturation is debatable because field observations suggest that localized strains can lead to high joint densities well beyond the proposed "saturation" levels (e.g. Becker and Gross, 1996; Gross et al., 1997). If these observations are applicable to the assessment of saturation, commonly observed thickness-spacing ratios may simply reflect the relatively low joint-normal effective tensile stresses that predominate in most settings.

1.2. Joint trends as indicators of stress field orientations

Previous regional studies (e.g. Sbar and Sykes, 1973; Zoback and Zoback, 1980, 1989; Zoback, 1992; Eyal, 1996) reveal that (1) intraplate stresses can originate due to movements along remote plate boundaries, (2) large plate-scale regions can be subjected to a uniformly oriented stress field, and (3) regional stress provinces can be identified, delineated, and related to regional active tectonic processes. Regional stress analysis based on geological data incorporates structures of all scales. Specifically, joints are opening-mode fractures that propagate in the plane of σ_1 and σ_2 and normal to σ_3, and thus are sensitive indicators of the local stress field orientation (Dyer, 1988; Pollard and Aydin, 1988). Because vertical joints, dyke patterns (Muller and Pollard, 1977) and systematic joints (Engelder and Geiser, 1980) align parallel to the trend of the maximum horizontal stress (S_H), they are used to construct regional paleostress trajectories. Furthermore, late-formed joints are often aligned parallel to the regional trend of the contemporary tectonic stress (modern-day S_H), and are thus used for mapping the orientation of neotectonic stress fields (Engelder, 1982; Bevan and Hancock, 1986; Hancock and Engelder, 1989; Hancock, 1991; Gross and Engelder, 1991; Eidelman and Reches, 1992). In this paper, we define a "joint set" as a group of joints that share a common orientation, which suggests that they developed within the same stress field. As demonstrated in this study, joint sets with similar orientations could actually form at different times.

The primary goals of this study are to (1) use the joint spacing–layer thickness relationship as an indicator of relative strain associated with regional stress fields, and (2) to use the orientations, abutting and cross-cutting relations of joint sets to confirm the orientation and sequential development of neotectonic stress fields in southern Israel.

2. Geological setting

The outcrops selected for analysis belong to the flat-lying Gerofit Formation located within the southern flank of the Neqarot syncline (Fig. 1). Nahal Neqarot is a large dry river in the central Negev of Israel, situated along the axis of the Neqarot syncline. The Neqarot syncline and the Ramon anticline to its immediate north are ENE–WSW-trending structures belonging to the arcuate Syrian Arc fold belt (Krenkel, 1924; Bentor and Vroman, 1954) that extends from northern Sinai through Israel and into Syria (Fig. 1a). An erosional cirque (Makhtesh) has developed around the axis of the Ramon anticline. The left-lateral Dead Sea transform (DST), which marks the plate boundary between the African and Arabian plates, is found east of the Ramon anticline. A rift valley has developed along the DST due to a change from pure strike-slip to transtensional motion (Garfunkel, 1981; Joffe and Garfunkel, 1987). The Ramon fault zone is located along the southern, steep to locally overturned flank of the Ramon anticline and extends from central Sinai to the rift valley. Garfunkel (1964), Bartov (1974), and Baer and Reches (1989) interpreted the Ramon fault zone as an oblique right-lateral strike-slip fault with as much as 700 m and 2.5 km of reverse and horizontal displacement, respectively. Alternatively, Becker (1994) interpreted this fault zone as a system of normal and reverse fault segments whose overall geometry suggests the presence of a blind reverse fault at depth without significant strike-slip motion. The Arif Bator fault zone parallels the Ramon fault about 10 km to the south, but its influence on fracture development in the study area is negligible.

The stratigraphic section of the western Neqarot syncline is comprised mainly of the Upper Turonian Gerofit Formation overlain by the Senonian Menuha and Mishash Formations (Ben-David, 1992, Becker, 1994). The Mishash Formation is comprised of alternating cherts, minor chalks, and limestone layers, whereas the Menuha Formation consists mainly of massive white chalks (Bentor and Vroman, 1960, Ben-David, 1992). The Gerofit Formation consists of well-bedded (10–60 cm thick) limestones and marly to chalky limestones interbedded with thin marl layers. The combination of extensive exposures of the Gerofit formation along Nahal Neqarot, thin to medium bed thicknesses, and a mechanical stratigraphy consisting of alternating jointed and non-jointed beds provides an excellent opportunity to investigate a variety of issues related to joint development in layered rocks.

3. Regional stress fields in southern Israel

At any one time and locality, the existing stress tensor is comprised of the sum of stress tensors resulting from various sources, remote, regional and local. The trend and intensity of this regional stress tensor may vary due to a change, in time and space, of its various components. The structures in southern Israel suggest that the orientation of tectonic stress has changed several times since the late Cretaceous. Initiation of Syrian Arc folding in the late Cretaceous reflects either a NW–SE S_H (Garfunkel, 1981;

Garfunkel and Bartov, 1977) or a WNW–ESE S_H (Letouzey and Tremolieres, 1980; Eyal and Reches, 1983; Eyal, 1996). We believe the WNW–ESE S_H trend is more appropriate because: (1) it is compatible with stress indicators measured in the western and north-central part of the African plate in general (Zoback, 1992), and in the Sinai–Israel plate in particular; (2) Eyal and Reches (1983) and Eyal (1996) concluded, based on 165 sites spread over the Sinai–Israel sub-plate, Jordan and Syria, that the WNW–ESE trend better explains the Turonian to Recent structures; and (3) as will be shown in this paper, the WNW–ESE trend is common among joint sets in the study area. The development of the Dead Sea transform during the middle Miocene (Bartov et al., 1980; Eyal et al., 1981; early Miocene according to Letouzey and Tremolieres, 1980) is associated with a second trend of compression, with S_H aligned NNW–SSE, that overprints the region (Eyal and Reches, 1983). The older stress field (WNW–ESE S_H) is known as the Syrian Arc stress field (SAS) and the younger stress field (NNW–SSE S_H) is known as the Dead Sea stress field (DSS) (Eyal and Reches, 1983) (Fig. 1a).

In accordance with the Zoback (1992) model the SAS, which is compatible with motion of the African plate relative to the Mid-Atlantic Ridge, is regarded as a remote stress field, whereas the DSS, which is associated with the motion along the DST, is regarded as a regional stress field. In light of young meso- and macrostructures that reflect the presence of both stress regimes since the Miocene, Eyal (1996) proposed a modified model whereby the regional stress field since the Miocene consists of the DSS superimposed on the more remote regional, plate-scale, SAS (Fig. 1a). Earthquakes corresponding to the DSS are far more numerous and have greater magnitudes than earthquakes associated with the SAS. This suggests a greater intensity for the DSS, and suggests the orientation of the regional stress during interseismic periods is mainly controlled by the DSS as strain accumulates along major faults in the region. However, one consequence of relaxation after major earthquakes is that the magnitude of the DSS drops so that the orientation of the regional stress field adjacent to the DST is controlled by the more persistent SAS.

Our objective is to identify joint set trends in Nahal Neqarot and compare their mean strikes with the trends of the two regional stress fields. This exercise may shed light on whether joint propagation in Nahal Neqarot is a consequence of these two regional stress fields, or whether their propagation reflects local stress perturbations associated with movement along the Ramon fault zone or development of the Ramon anticline. Uniform joint set trends aligned parallel to documented regional S_H would suggest the former (e.g. Engelder and Geiser, 1980), whereas dramatic changes in joint trends over short distances would suggest the latter (Rawnsley et al., 1992). In addition, age relationships among joint sets may clarify whether joint development is a manifestation of the Eyal (1996) model for a weak remote stress field characterized by temporal variations in stress orientation and magnitude due to stress accumulation and release on the DST.

4. Method of data collection

Joint orientation data (strike and dip) were collected at 34 stations in the flat-lying Gerofit Formation along the Neqarot River, south of the Ramon monocline (Fig. 1b, c). One to three beds were measured at each station depending upon the quality of exposure. Jointing lithologies are classified as limestones, chalky limestones, and marly limestones based on field inspection. Joint orientations were measured in a total of 50 beds, with each bed containing anywhere from one to three joint sets (Table 1). To ensure statistically robust mean joint orientations, we measured 30–40 joint orientations for each joint set in each bed and processed the data with Richard Allmendinger's Stereonet 4.9.6 program. Rotation of bedding to the horizontal position is not necessary because the regional dip does not exceed a few degrees, and more than 90% of the joints in this area are sub-vertical and perpendicular to bedding. The majority of the joints lack any surface structures such as plumose structures or mineralization. On a few joint surfaces we observed striations which supposedly developed due to later movement along the joints. The systematic joint sets could be followed, in plan-view, for several meters according to the size of the exposure. Abutting and cross-cutting relations (e.g. Hancock, 1985; Dunne and North, 1990) along with curving geometries (e.g., Dyer, 1988) were used to determine the relative timing of joint set formation within each bed.

A total of 28 joint-spacing scanlines were measured across first generation joints in various lithologies (Table 2). Spacing data from only the first-formed joint set in each bed were collected to avoid effects of pre-existing joints on subsequent joint development, and measurements were not taken adjacent to throughgoing fault or fracture zones to minimize local strain effects (Bahat, 1988; Becker and Gross, 1996). Joint spacing was calculated as the perpendicular distance between adjacent joints belonging to the same set, and a minimum of 40 spacing measurements were taken along each scanline wherever possible. In addition, we measured the MLT for each bed, which in layered rocks is defined as the thickness of the mechanical unit that controls joint height (Gross et al., 1995). We also include the Nahal Neqarot joint-spacing data of Becker and Gross (1996) in Table 2 and subsequent analysis.

5. Results and analysis

5.1. Joint set orientations and relative timing of their formation

Joint orientations for each station are presented as rose

Table 1
Summary of joint orientation data from Nahal Neqarot by station and bed number[a]

		First set				Second set				Third set			
Station	Lithology	Strike	Dip	$\alpha 95$	Stress field	Strike	Dip	$\alpha 95$	Stress field	Strike	Dip	$\alpha 95$	Stress field
5 bed 1	m. lst	146	87	3	DSS								
5 bed2	m. lst	152	90	2.3	DSS								
6	lst	153	87	4.6	DSS								
7	lst	158	84	3.5	DSS								
8 bed 1	lst	165	85	11.6	DSS								
8 bed 2	ch. lst	165	90	3	DSS								
9 bed 1	lst	168	88	2.1	DSS								
9 bed 2	lst	111	90	3.5	SAS								
10 bed 1	ch. lst	106	90	1.7	SAS	161	90	2.2	DSS				
10 bed 2	lst	121	90	2.1	SAS								
11	m. lst	164	90	1.9	DSS								
12	m. lst	140	90	1.1	NW–SE	167	90	1.6	DSS	111	90	1.4	SAS
13 bed 1	lst	167	85	1.6	DSS	117	90	3.5	SAS	87	86	3.5	SAS
13 bed 2	m. lst	166	79	1.6	DSS								
13 bed 3	m. lst	165	79	1.7	DSS								
14 bed 1	lst	163	90	1.5	DSS								
14 bed 2	m. lst	97	90	4.2	SAS								
15	lst	154	90	1.2	DSS	100	90	1.7	SAS				
16	lst	88	90	1.1	SAS	145	90	2.8	DSS				
17 bed 1	lst	113	90	2.6	SAS	23	90	2.8	NE–SW				
17 bed 2	lst	62	90	2.2	NE–SW	133	90	2.7	NW–SE				
18	lst	107	90	1	SAS	164	90	3	DSS	22	90	1	NE–SW
19	lst	105	90	2.4	SAS	170	90	2	DSS				
20	lst	108	90	1.7	SAS	184	90	1.4	DSS				
21	lst	156	87	2	DSS	134	90	3.9	NW–SE				
22 bed 1	lst	155	85	1.7	DSS								
22 bed 2	ch. lst	125	90	1.3	SAS								
23 bed 1	ch. lst	153	88	2.5	DSS								
23 bed 2	ch. lst	157	81	2.2	DSS								
24 bed 1	lst	160	81	2.5	DSS								
24 bed 2	lst	136	85	2.2	NW–SE	163	90	1.6	DSS				
25 bed 1	lst	132	85	1.6	NW–SE	160	90	1.2	DSS				
25 bed 2	ch. lst	166	90	1.7	DSS								
25 bed 3	ch. lst	126	90	2	NW–SE	160	85	1.4	DSS				
26	lst	180	86	1.6	DSS	118	90	1.2	SAS				
27	lst	47	90	1.1	NE–SW	157	90	1.2	DSS				
28	lst	148	90	1.7	DSS	24	90	2	NE–SW	107	90	0.9	SAS
29	lst	113	90	3.0	SAS	157	88	2.5	DSS				
30	n.d.	161	90	1.4	DSS								
31	m. lst	125	89	1.1	SAS	31	90	1	NE–SW				
32	lst	155	90	1.6	DSS								
M-1	ch. lst	103	75	2.5	SAS								
M-2 bed 1	ch. lst	155	90	2.4	DSS								
M-2 bed 2	lst	111	90	2.2	SAS								
M-3 bed 1	n.d.	160	90	1.7	DSS								
M-3 bed 2	n.d.	36	90	1.9	NE–SW								
M-3 bed 3	n.d.	160	90	2.4	DSS								
M-4	n.d.	152	90	3.9	DSS	115	90		SAS				
A-1 7 Jan	n.d.	169	90	1.8	DSS	44	90	5.4	NE-SW				
M-3 7 Jan	n.d.	159	90	1.1	DSS	39	90	4.7	NE-SW				

[a] Included for each bed are lithology and mean orientation (strike, dip, $\alpha 95$, compatible stress field) for each set according to its relative timing of formation. ch. lst, chalky limestone; lst, limestone; m. lst, marly limestone; n.d., not determined. $\alpha 95$, the radius of confidence cone of Fisher vector distribution. It implies the probability that the mean trend is located within the given small circle at a confidence of 95%.

diagrams and are plotted according to their geographic position (Fig. 2). In cases where joint set orientations differed markedly between adjacent beds at the same station (Station 17, Station M-3), separate rose diagrams are provided for each bed. The abundant joint orientations are correlated with the appropriate S_H orientation of the appropriate stress field. The entire population of joints at Nahal Neqarot can be divided into four main sets based on

Table 2
Summary of spacing data and statistics for first-formed joints measured in Nahal Neqarot[a]

Station	Lithology	Mean strike of joint set	Stress field	Stand. Dev.	Mean spacing (cm)	Median spacing (cm)	Mean MLT (cm)	FSR	No. of spacing measurements
5 bed 1	m. lst	146	DSS	5.8	17.0	16.0	54.5	3.40	40
5 bed 2	m. lst	152	DSS	1.23	3.2	3.0	19.4	6.47	42
6	lst	153	DSS	11.05	18.0	15.0	17.0	1.14	41
7	lst	158	DSS	9.06	20.6	19.0	25.0	1.32	40
8 bed 1	lst	165	DSS	7.6	17.6	16.0	23.0	1.44	40
8 bed 2	ch. lst	165	DSS	5.39	10.6	8.8	26.4	3.02	40
9 bed 1	lst	168	DSS	11.33	23.8	22.3	25.5	1.15	40
13 bed 1	lst	167	DSS	6.39	15.2	13.8	12.4	0.90	40
13 bed 2	m. lst	166	DSS	3.24	7.5	7.3	35.7	4.92	40
13 bed 3	m. lst	165	DSS	2.16	7.1	7.0	28.8	4.12	40
21	lst	156	DSS	4.6	14.5	13.5	29.4	2.18	40
22 bed 1	lst	155	DSS	3.4	7.9	7.8	20.7	2.67	40
23 bed 1	ch. lst	153	DSS	6.02	12.0	10.5	19.5	1.86	40
23 bed 2	ch. lst	157	DSS	3	5.0	4.5	31.7	7.04	40
24 bed 1	lst	160	DSS	2.66	6.6	8.0	31.6	3.94	40
24 bed 2	lst	136	NW	3.36	8.8	8.0	11.4	1.43	40
25 bed 1	lst	132	NW	6.92	18.5	17.5	19.1	1.09	40
25 bed 2	ch. lst	166	DSS	2.57	6.3	6.3	30.5	4.88	33
26	lst	180	DSS	8.33	16.0	15.3	17.4	1.14	41
29	lst	113	SAS	19.01	40.0	37.0	30.9	0.84	29
B & G-I	lst	113	SAS	14.96	23.7	21.1	18.0	0.85	110
B & G-II	lst	113	SAS	7.76	13.8	12.7	18.0	1.42	237
B & G-III	lst	113	SAS	9.31	14.4	13.0	18.0	1.38	271
B & G-IV	lst	113	SAS	12.85	20.7	18.0	18.0	1.00	94
M-1	ch. lst	103	SAS	5.92	13.6	13.0	18.0	1.38	80
M-2 bed 1	ch. lst	155	DSS	2.45	5.2	5.0	37.0	7.40	48
M-2 bed 2	lst	111	SAS	8.19	5.4	13.0	19.0	1.46	13
M-3 bed 1	n.d.	160	DSS	4.07	11.7	12.0	35.0	2.92	9
M-3 bed 2	n.d.	036	NE	7.49	22.3	21.0	15.0	0.71	22
M-3 bed 3	n.d.	160	DSS	3.08	7.2	7.0	14.8	2.11	17
M-4	n.d.	152	DSS	18.1	22.8	18.0	24.9	1.38	8
M-3 7	n.d.	159	DSS	12.2	19.2	17.0	12.4	0.73	48

[a] B & G, data from Becker and Gross (1996); FSR, Fracture Spacing Ratio; MLT, Mechanical Layer Thickness. Refer to Table 1 for other abbreviations.

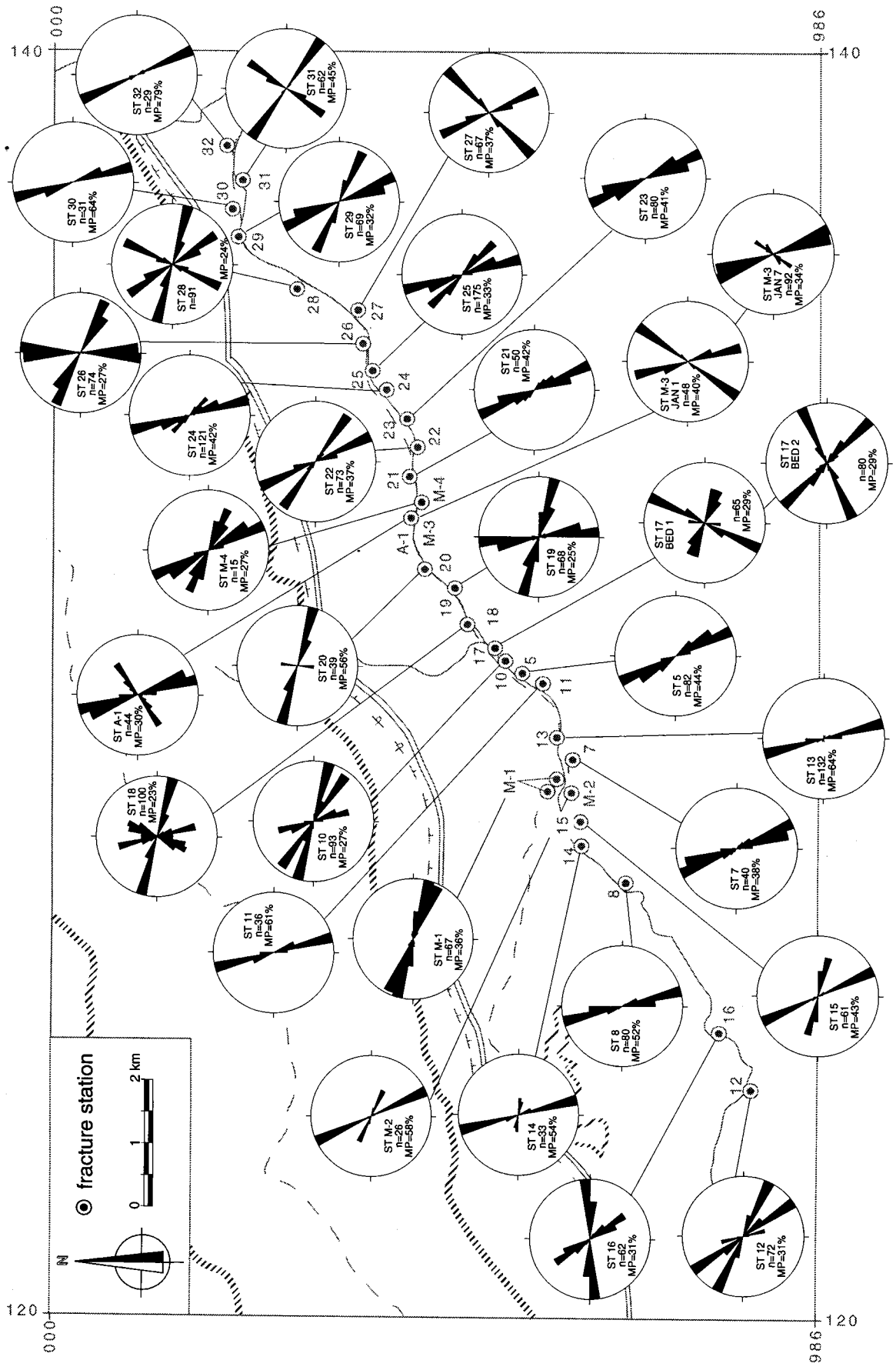

Fig. 2. Rose diagrams of joint orientations at each station. Unless otherwise indicated, each rose diagram consists of data from all beds at an individual station. Number of joints (n) are indicated within each rose diagram, as is the maximum percentage (MP) marking the perimeter. Sector size is 10°.

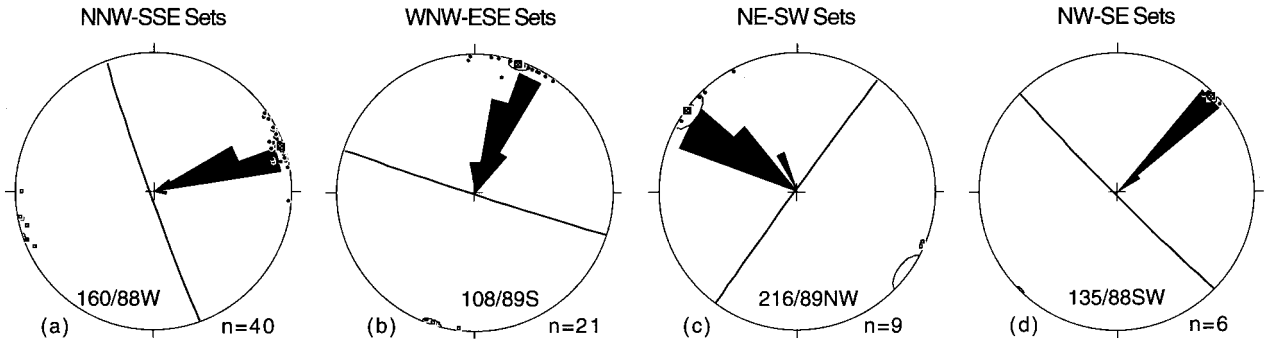

Fig. 3. Summary equal area stereographic projections of the four main joint trends at Nahal Neqarot. Each data point (i.e. pole) is the mean orientation for a single set of systematic joints within an individual bed (Table 1). The mean orientation for each combined plot is a great circle whose pole is represented by a square. Rose petals indicate the relative frequency of the poles. (a) NNW–SSE sets (DSS compatible). (b) WNW–ESE sets (SAS compatible). (c) NE–SW sets. (d) NW–SE sets. Rose sector size is 10°.

orientation (Fig. 3):

(a) A joint set with a mean strike of 160–340° and $\alpha_{95} < 3°$ found in 40 beds at 32 stations.
(b) A joint set with a mean strike of 108–288° and $\alpha_{95} < 5°$ found in 21 beds from 19 stations.
(c) A joint set with a mean strike of 036–216° and $\alpha_{95} < 9°$ found in nine beds at eight stations.
(d) A joint set with a mean strike of 136–316° and $\alpha_{95} < 6°$ found in six beds at five stations.

Several general observations are apparent from inspection of the rose diagrams. First, the predominant trend is NNW–SSE, with other trends at WNW–ESE, NW–SE, and NE–SW. Second, joint set orientations vary among the stations without consistent spatial trends. For example, the NNW–SSE set is present in Station 32, yet absent in neighboring Station 31. The NW–SE set is found at opposite ends of the study area (Stations 12 and 31), yet is absent from many stations in between (e.g. Stations 13, 19, and 27). Third, the number of joint sets at each station is variable, ranging from one set (e.g. Stations 11 and 23) to four sets (Station 17). Fourth, in stations where joints from more than one bed were measured, the same systematic set is not necessarily found in all beds. Sometimes, joints in adjacent beds have similar orientations (e.g. NNW–SSE in beds 1 and 2 of Station 8; Table 1), whereas at other stations the NNW–SSE set is found in one bed and the WNW set is found exclusively in the other bed (e.g. Stations 9, 14, and 22).

Relative ages of joint sets, in layers that include more than one joint set, is determined by fracture abutments, cross-cutting relationships, and curving geometries. A long and continuous joint set is defined as the systematic, first formed set. A joint set that fractures the rock between the systematic set and abuts the planes of the systematic set is regarded as the second joint set. Sometimes a few of the joints of the second set succeed in crossing one or a few joints of the older joint set (Fig. 4). In only a few cases, we could not determine the age relationships because the abutting was inconclusive.

A younger fracture may terminate against a pre-existing fracture in a variety of geometries (e.g. Hancock, 1985). Orthogonal joint sets typically display "T" intersections where joints belonging to the younger set terminate at right angles to the pre-existing joints. Where two joint sets are not orthogonal to each other, the joints may form angular intersections (e.g. the "Y" intersection of Hancock, 1985). As a result of local stress perturbations caused by pre-existing joints, many joints belonging to a younger set will curve as they approach older joints. The "curving parallel" and "curving perpendicular" geometries of systematic cross-joints are examples of this behavior (Dyer, 1988). All of the above-mentioned abutting and curving geometries were observed in the study area. Relative ages for joint sets within a given bed were characterized as conclusive where 95–100% of abutments and curving geometries revealed consistent timing relationships. A typical example of joint terminations and intersection geometries observed on a bedding surface is presented in Fig. 5.

Unlike other localities where one joint set of a given orientation consistently predates another joint set (e.g. Dyer, 1988; Srivastava and Engelder, 1990; Rawnsley et al., 1992), at Nahal Neqarot there is no consistent trend for the first-formed joint set in cases where more than one set of joints is found in a single bed. For example, in beds at Stations 10 (bed 1), 18, 19, and 29, the trend of the first-formed joint set is WNW–ESE, whereas the second-formed joint set trends NNW–SSE (Table 1). In contrast, in beds at Stations 12 (the second and third joint sets), 13 (bed 1), 15, 26, 28, and M-4 the formation of the NNW–SSE joint set predates the formation of the WNW–ESE set. Similar inconsistencies in timing are observed for the less abundant NW–SE and NE–SW joint sets. In beds at Stations 12, 24 (bed 2), and 25 (beds 1 and 3) the NW–SE set is first to form and predates the NNW–SSE set, whereas at Station 17 (bed 2) the NE–SW set predates the NW–SE set. At Station 21 the NW–SE joint set postdates the NNW–SSE set. Similarly,

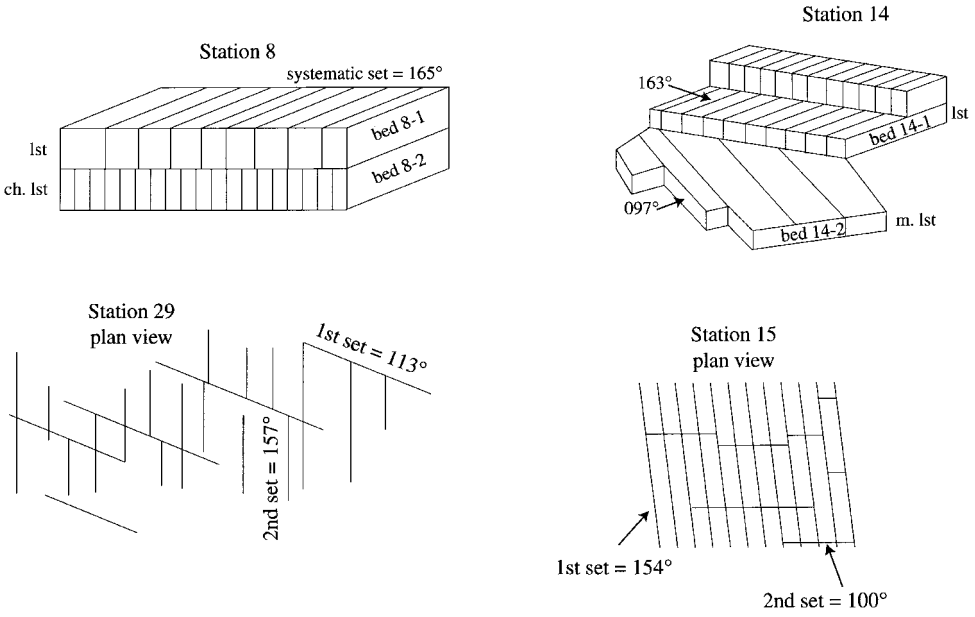

Fig. 4. Sketches of typical joint patterns observed in outcrops of the Gerofit Formation in Nahal Neqarot showing general abutting relations and differences in spacing and trends between beds at the same station.

joints belonging to the NE–SW set are the first to form in beds at Stations 17 (bed 2) and 27, but are the second or third set of joints to form in beds at Stations 17 (bed 1), 18, 28, 31, A-1, and M-3 (Jan). Of the 28 beds in which only one joint set was observed, the NNW–SSE set is found in 21 beds, the WNW–ESE set appears in six beds, and the NE–SW set is found in one bed.

The 160–340°-trending joint set (Fig. 3a, representing 52% of the entire dataset) propagated parallel to S_H of the DSS and is approximately normal to the trend of the Ramon anticlinal axis and the Ramon fault zone (Fig. 1a, b). The 108–288° joint set (Fig. 3b, representing 28% of the entire dataset) propagated parallel to S_H of the SAS. Joints belonging to these two sets comprise 80% of the entire dataset of mean joint set orientations. Independent evidence for the existence of SAS in the area south of the Ramon structure include: (1) many mesostructures measured by Eyal and Reches (1983) just east of the present study area; (2) about 10 sub-horizontal tectonic stylolites whose teeth trend WNW–ESE to E–W (e.g. Stations 18 and 20); (3) three small normal faults (e.g. Stations 10 and 17); and (4) the right-lateral movement along the Ramon fault. Joints trending NW–SE and NE–SW (i.e. the 135–315° and 216–036° sets; Fig. 3c, d) were found in only six and nine beds, representing 8% and 12% of the entire dataset, respectively.

In light of their parallel alignment with S_H of established regional stress fields, we conclude that the NNW–SSE joint set propagated under conditions associated with the DSS, whereas the WNW–ESE joint set propagated under conditions associated with the SAS. The stress fields responsible for the NW–SE and NE–SW joint sets are not apparent to us, but their abundance is much less then the other two sets. The NW–SE-trending joint set could have formed while the cumulative DSS and SAS stress fields resulted in a NW–SE S_H. Alternatively, both NW–SE and NE–SW joint sets may represent local stresses associated with the Ramon fold and/or fault zone. About 65 km to the north near Beer Sheva, Bahat (1986, 1987, 1999) described several bed-confined joint sets in Eocene chalks. He related the NW ("cross fold") and ENE ("strike") joint sets to local

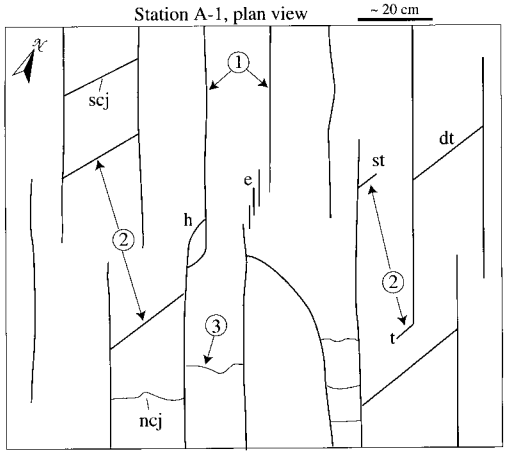

Fig. 5. Sketch of joint terminations and intersection geometries at Station A-1. Numbers refer to relative timing of joint sets. Note the first-formed set in this bed is NNW–SSE (1), the second-formed set trends NE–SW and is comprised of systematic cross-joints (scj; 2), and the third-formed set consists of non-systematic cross-joints (ncj; 3). Labeled geometries are echelon (e), hooking (h), tilt (t), single termination (st), and double termination (dt).

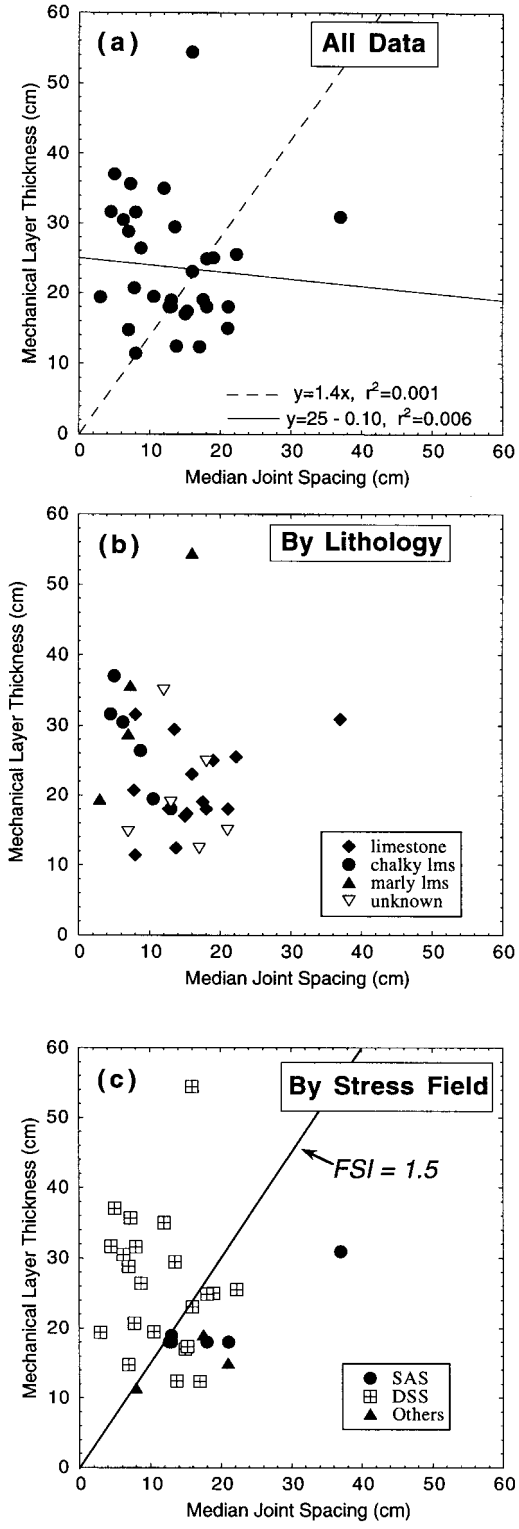

Fig. 6. Fracture spacing index (FSI) plots for first-formed joints at Nahal Neqarot. (a) All data. Note lack of correlation between joint spacing and layer thickness. Correlations are for best-fit line and best-fit line fixed through the origin. (b) All data identified by lithology. (c) All data identified according to interpreted prevailing stress field. FSI line of 1.5 is plotted for reference.

fold development due to their orthogonal and parallel alignment with respect to fold axes.

The most pervasive joint set formed in conjunction with the DSS, as 80% of all beds contain a joint set aligned NNW–SSE. Forty-two percent of beds contain joints that propagated under the influence of the SAS, whereas joints corresponding to other stress fields are less abundant. Abutting relations of joints within individual beds, among beds at the same outcrop, and among beds at different localities demonstrate that joint sets were alternatively active. These age relationships of various joint sets imply that the regional stress field fluctuated through time, mostly between a NNW-trending S_H of the DSS and a WNW-trending S_H of the SAS.

5.2. Joint spacing as a function of layer thickness, lithology, and joint trend

The relationship between joint spacing and mechanical layer thickness may be quantified using the fracture spacing index (FSI) of Narr and Suppe (1991) or the fracture spacing ratio (FSR) of Gross (1993). The FSI is defined as the slope of the best-fit line when joint spacing (x-axis, dependent variable) is plotted versus mechanical layer thickness (y-axis). The FSI yields a single characteristic value of joint intensity for numerous jointed beds of varying thicknesses. The FSR is defined as the mechanical layer thickness divided by the median joint spacing for an individual bed. The FSR is useful for documenting changes in joint intensity within individual beds, comparing joint intensities among individual beds belonging to the same population, and for deriving a value of joint intensity relative to layer thickness for datasets where the range of layer thicknesses is limited. Higher values of FSI and FSR correspond to more closely spaced joints (i.e. higher joint densities). In cases where joint spacing correlates strongly with layer thickness, the FSI and FSR are nearly equal (Gross et al., 1995).

Fracture spacing index plots are presented as both combined datasets (Fig. 6) and as individual plots according to lithology (Fig. 7). Where appropriate, two linear regression lines are plotted through the data: one is the best-fit line and the other is forced through the origin (the FSI line). When all of the data are plotted together (Fig. 6a) two general results are apparent. First, there is no correlation between median joint spacing and layer thickness for the combined dataset as manifested by extremely low linear correlation coefficients, and, second, many data plot close to the vertical axis, indicating relatively high fracture spacing ratios (>2). This is in marked contrast to the results reported by Narr and Suppe (1991) of a strong layer thickness–joint spacing correlation for all lithologies combined together, and for a uniform FSI of $\sim$1.5. Furthermore, joint spacing in marly limestones and chalky limestones is always less than 16 cm regardless of mechanical layer thickness, whereas joint spacing in limestone ranges up to 36 cm (Fig. 7).

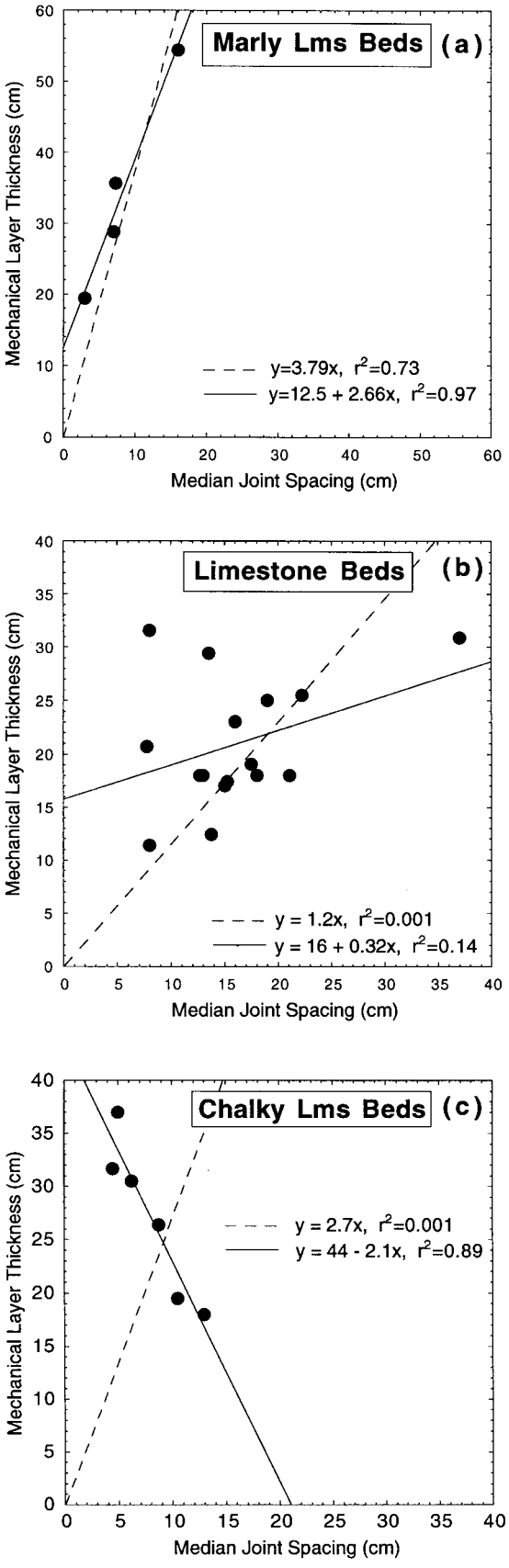

Fig. 7. Fracture spacing index (FSI) plots for first-formed joints according to lithology. Correlations are for best-fit line and best-fit line fixed through origin. (a) Marly limestones. (b) Limestones. (c) Chalky limestones.

Examination of spacing data at Nahal Neqarot by lithology reveal that, as a general rule, joints in the marly limestones and chalky limestones are more closely spaced relative to layer thickness than joints in pure limestones: mean FSRs for marly limestones, chalky limestones, and pure limestones are 4.7, 4.25 and 1.44, respectively (Table 2). Differences in joint spacing relative to layer thickness as a function of lithology were reported by Ladeira and Price (1981) and Gross et al. (1995). However, thickness–spacing plots for each lithology do not follow commonly observed trends in the literature. In marly limestone beds, joint spacing correlates strongly to layer thickness, with an FSI of 3.8 for the regression line fixed through the origin. A higher correlation and shallower slope is derived for the best-fit unconstrained line (Fig. 7a). For limestone beds, there is no correlation between joint spacing and mechanical layer thickness (Fig. 7b). The thickness–spacing plot of chalky limestone beds (Fig. 7c) is especially unusual in light of its negative slope, which indicates that joint spacing is wider in thinner beds, in contrast to most joint spacing data in the literature that show wider spacing in thicker beds (e.g. Ladeira and Price, 1981; Engelder et al., 1997).

The lack of correlation between joint spacing and layer thickness for most data implies that mechanical layer thickness does not exert an overriding dominant influence on joint spacing in Nahal Neqarot. Furthermore, the exceptionally wide scatter in the limestone plot (Fig. 7b), as well as the unusual negative slope for the chalky limestone beds (Fig. 7c), indicate that lithology alone is not responsible for the overall scatter in observed joint spacing. One possible explanation for this result is that the joint spacing–layer thickness relationship, though perhaps most pronounced in rocks with high competency contrasts, is less pronounced or even absent for rocks with small competency contrasts, such as the carbonates of the Gerofit Formation. Although we cannot rule out this possibility, we have observed strong spacing–layer thickness correlations in other outcrops of similar lithologies (e.g. Becker and Gross, 1996; Gross et al., 1997). Furthermore, when FSR values for all beds are plotted in a histogram, the NNW-trending joint sets span a wide range, whereas all other trending joint sets have FSR values close to 1 (Fig. 8). Fracture spacing ratios of the non-NNW-trending joints fall within typical ranges reported in the literature (e.g. Narr and Suppe, 1991; Gross, 1993; Engelder et al., 1997; Gross et al., 1997; Ji and Saruwatari, 1998; Bai and Pollard, 2000), suggesting that spacing of these joint sets roughly correlates to layer thickness. The deviation in FSR solely for the NNW-trending joints suggests to us the presence of another boundary condition unique to this trend.

Therefore, in an effort to identify other factors that may have influenced joint spacing in Nahal Neqarot, we plotted

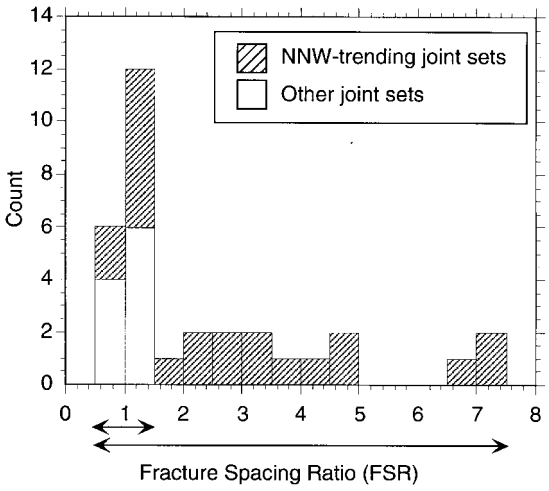

Fig. 8. Histogram of the FSR according to joint trend for all first-formed joint sets measured in Nahal Neqarot. Note wide range and large FSR values for NNW-trending joint sets.

the spacing data according to the interpreted prevailing stress field in which they formed, with NNW joint trends belonging to the DSS, WNW trends belonging to the SAS, and the remaining trends grouped as "others" (Fig. 6c). The resulting plot reveals a remarkable pattern: without exception, all points that plot above the FSI = 1.5 line (proposed "saturation" level) correspond to joints that developed within the DSS regime, whereas all joints that formed during the SAS or other stress regimes fall beneath this line (Fig. 6c). When considered according to lithology, joints in all four marly limestone beds belong exclusively to the DSS set, whereas joints in five of the six chalky limestone beds also belong to the DSS set (compare Fig. 6c with Fig. 7a and c). On the other hand, joints in limestone beds are more equally balanced between the DSS and other stress fields (compare Fig. 6c with Fig. 7b). Furthermore, the three notable exceptions of FSR greater than 2.0 for limestones mentioned above all correspond to joints belonging to the DSS regime. Therefore, whereas marly limestone and chalky limestone beds undergo brittle deformation in response to the Dead Sea stress regime, they mostly do not fracture as a result of Syrian Arc and other stresses. Furthermore, joints belonging to the DSS (mean FSR = 2.99) generally have higher FSR than joints belonging to the SAS (mean FSR = 1.12) or to other stress fields (mean FSR = 1.07).

5.3. Normalized joint spacing histograms

Many researchers have observed a regular spacing for joints belonging to an individual set (e.g. Gillespie et al., 1993). Joint spacing histograms may reveal important aspects of the fracturing process, such as the degree of joint set development and the influence of flaws on fracture distributions (Huang and Angelier, 1989; Narr and Suppe, 1991; Rives et al., 1992; Fischer, 1994; Becker and Gross, 1996; Ruf et al., 1998; Rabinovitch and Bahat, 1999; Gillespie et al., 1999). Histograms must contain large quantities of data to yield meaningful results; therefore, data from numerous beds are often combined together by normalizing joint spacings in each bed to its median value, thereby eliminating effects of layer thickness (Narr and Suppe, 1991; Gross, 1993; Ruf et al., 1998). Although the process of combining joint spacing from numerous beds in this manner may mask important differences, such as effects of localized strain (Becker and Gross, 1996), it may nonetheless reveal general trends that have significance. Normalized joint spacing histograms typically yield positively skewed distributions with a modal value of approximately 1.

We grouped joint spacing data from Nahal Neqarot according to the trends of the two dominant joint sets, the NNW set and the WNW joint set (Fig. 9). Spacing measurements were normalized in two ways: to the median joint spacing in each bed and to the mechanical layer thickness of the bed. Note that when joint spacing for the sets is normalized to the median spacing value (Fig. 9a, b), the distributions resemble the commonly observed positively skewed shape (i.e. a log-normal appearance). When joint spacing is normalized to mechanical layer thickness, the histograms have markedly different appearances. In contrast to the log-normal shape of the WNW sets histogram (Fig. 9d), the modal value of the NNW sets histogram is in the first bin interval, thus resembling a negative exponential distribution (Fig. 9c).

The character of normalized joint spacing distributions may reflect differences in the spacing of joints relative to layer thickness (normalized to MLT), as well as the regularity of joint spacing (normalized to median spacing). We illustrate these differences in Fig. 10. Each sketch consists of a thin bed (y) and a thick bed (x), with more closely spaced joints found in the thinner bed. Consider two pairs of beds where the joints are relatively evenly spaced: in one case the FSR is ~1 (Fig. 10a) and in the other case the FSR is ~2 (Fig. 10b). When normalized to median spacing the histograms will be similar to each other (Fig. 10a2, b2), with a unimodal distribution and a modal value of ~1. However, when normalized to MLT, the spacing distribution of beds with FSR ~2 will be confined to a narrower range and display a lower modal value than beds with FSR ~1 (Fig. 10a3, b3), reflecting the fact that joints are more closely spaced relative to layer thickness for higher FSR.

Applying these generalities to the results from Nahal Neqarot suggests the following. First, mechanically confined joints belonging to the NNW sets and WNW sets are relatively evenly spaced in light of the smooth, unimodal distribution when normalized to median joint spacing (Fig. 9a, b), similar to the conclusions of Narr and Suppe (1991), Ruf et al. (1998), and Gillespie et al. (1999). Second, joints compatible with the DSS (i.e. NNW sets) are considerably more closely spaced relative to layer thickness than joints compatible with the SAS (i.e. WNW sets), as manifested by

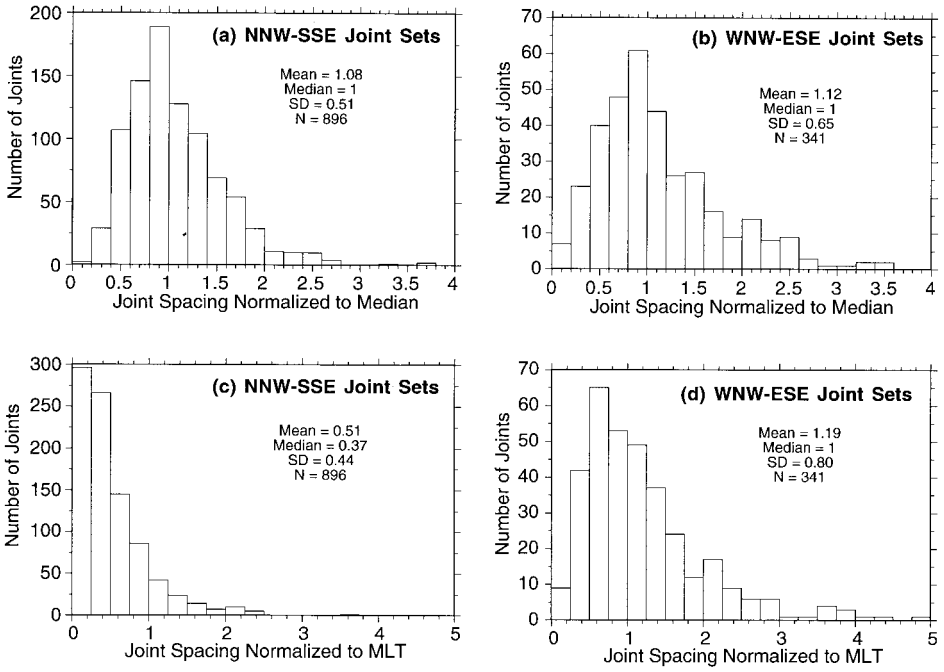

Fig. 9. Normalized joint spacing histograms according to orientation. Each joint spacing measurement is normalized either to the median spacing of the individual joint set for each bed (a, b) or to the mechanical layer thickness of the measured bed (c, d).

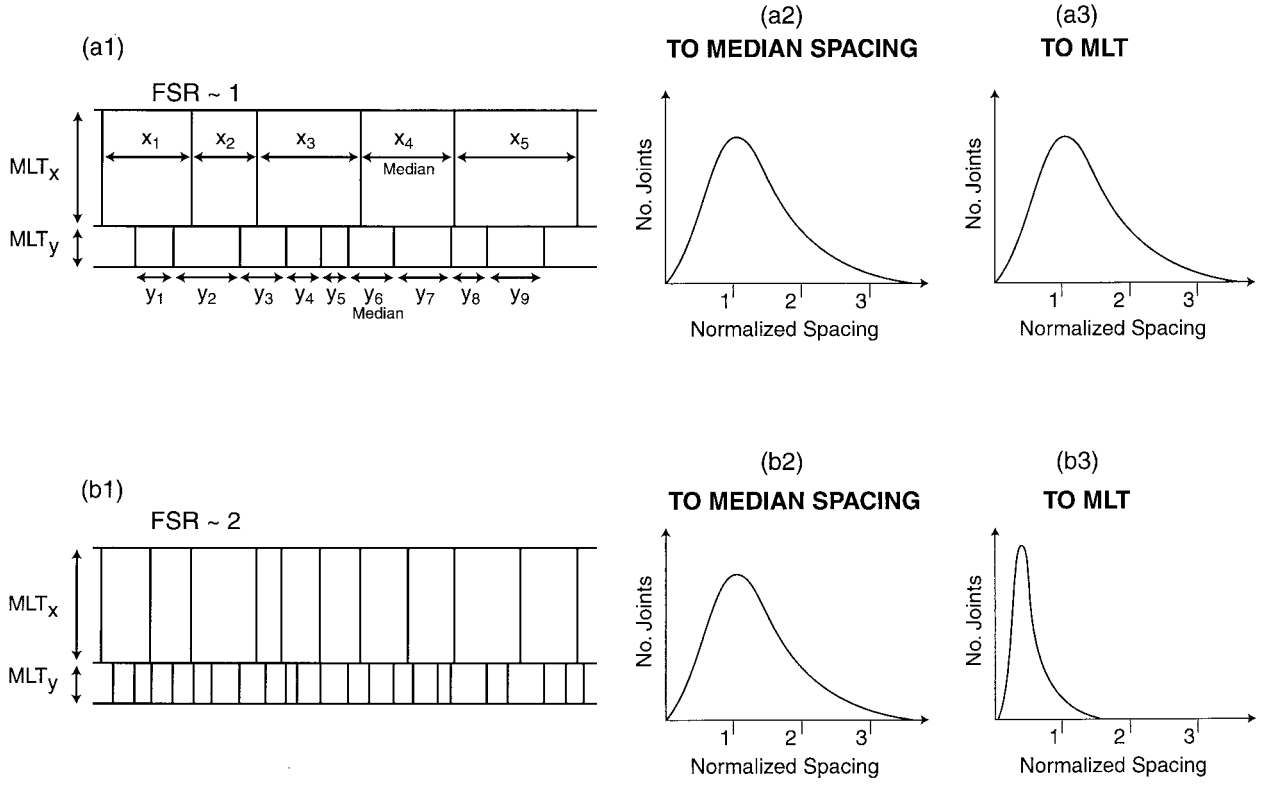

Fig. 10. Diagram of expected correspondence between mechanically confined joint pattern and normalized joint spacing distributions. When normalized to median joint spacing, a regularly spaced joint set will have a unimodal distribution with a peak at ~1 (a2, b2). When normalized to MLT, a regularly spaced joint set will display a single peak, although the position of the peak value along the horizontal axis will be a function of the FSR (a3, b3).

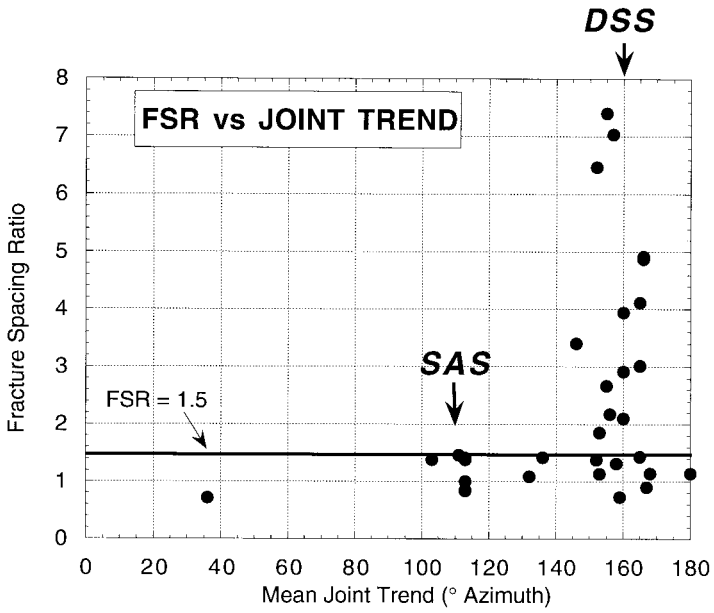

Fig. 11. Fracture spacing ratio (FSR) plotted as a function of mean azimuthal joint trend. Note that the highest FSR values are localized within the narrow range of 145–170°, corresponding to the trend of S_H of the DSS.

the markedly different distributions when normalized to MLT (Fig. 9c, d).

6. Discussion

6.1. FSR as an indicator of regional extension

Fractures generated in the laboratory (Garrett and Bailey, 1977; Rives et al., 1992; Wu and Pollard, 1995) and field studies (Becker and Gross, 1996) suggest that joint spacing decreases with increasing applied load, whether measured in terms of stress (Garrett and Bailey, 1977) or strain (Rives et al., 1992; Becker and Gross, 1996). New fractures form in between existing fractures through the process of "sequential infilling" (e.g. Hobbs, 1967; Narr and Suppe, 1991; Gross, 1993). Thus, in layered rocks where joints are confined to individual mechanical units, spacing may not only be a function of layer thickness and to a lesser extent lithology, but also a function of the amount of strain. This led Gross et al. (1997) to propose that the FSR could be used as an indicator of relative strain magnitude, especially in the vicinity of folds and fault zones.

Results from this study suggest that the FSR can also provide valuable information regarding regional strains, and consequently their causative regional stress fields. A plot of the FSR as a function of mean joint trend shows that, for all beds where first-formed joints are oriented between the 0° and 140° azimuth, the FSR is less than or equal to the commonly observed maximum value of 1.5 (Fig. 11). In contrast, for beds where joint trends fall between the 145° and 170° azimuth, seven beds exhibit FSR at or below 1.5; however, the FSR in 13 beds exceeds 1.5, with three of those beds displaying FSR greater than 6.0. The anomalously close joint spacings (i.e. high FSR) are restricted to a narrow range of joint trends, which in turn corresponds to the systematic joint set aligned NNW.

Joints and other fractures represent brittle strain that forms in response to an applied stress, often of tectonic origin (Holst and Foote, 1981; Hancock, 1985; Hancock et al., 1984; Engelder, 1985; Dunne and North, 1990). In compressional tectonic environments such as the Himalayas and Alps, shortening parallel to maximum compressive stress is accompanied by extensional strain normal to the trend of compression (e.g. Tapponnier et al., 1982; Selverstone, 1988). In the western Transverse Ranges of California, shortening has led to a large component (~10%) of along-strike extension accommodated by brittle jointing, opening-mode vein development, and normal faulting (Gross and Engelder, 1995).

A similar pattern between stress fields and regional strains was established for Israel and the Sinai since the Late Cretaceous. For both the SAS and DSS, there exists a suite of macro- and mesostructures that indicate regional shortening parallel to S_H, along with a simultaneous regional extension normal to S_H (Eyal and Reches, 1983; Eyal, 1996). Evidence for regional shortening includes fold axes, tectonic stylolites, reverse faults, and strike-slip faults, whereas evidence for regional extension normal to S_H includes normal faults, strike-slip faults, veins, and dikes (Fig. 12). The joints measured in this study are most probably a manifestation of the regional extension that took place in response to the SAS and DSS. The strain, along with other mechanisms such as elevated fluid pressures, may have contributed to a state of local effective tension that led to joint propagation. We propose that the

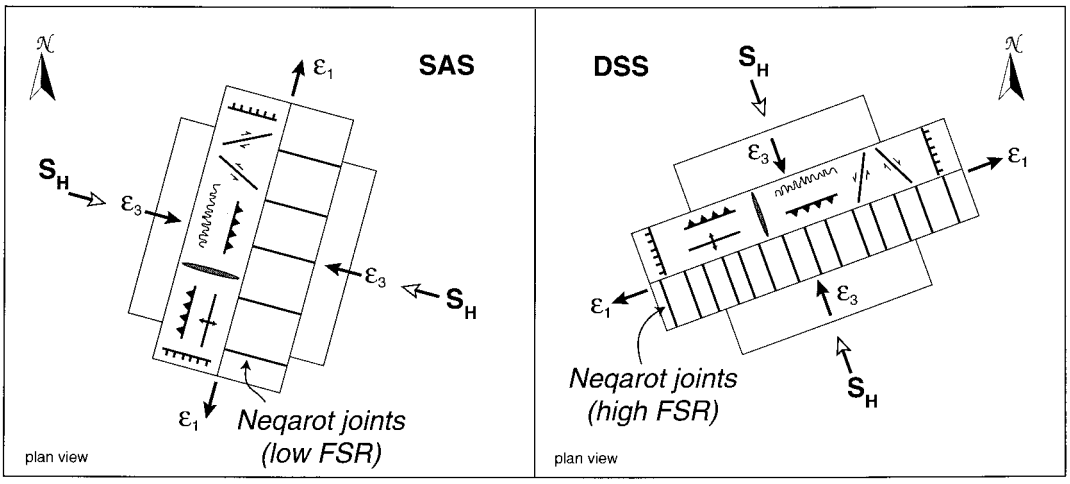

Fig. 12. Sketches showing the relationship between regional stress fields (S_H) and regional strains (ε_1, ε_3) from macro- and mesostructures observed by Eyal and Reches (1983) and Eyal (1996), along with joints measured in this study. Square represents undeformed original shape, and rectangle depicts relative amounts of shortening parallel to S_H and extension normal to S_H. The more closely spaced joints associated with the DSS (higher FSR) are interpreted to correspond to a greater magnitude of regional extension normal to S_H. ε_1 and ε_3 are the directions of maximum and minimum extension.

higher FSR measured for the NNW joint set reflects a greater amount of extensional strain than occurred in response to DSS compression (Fig. 12).

6.2. Model for neotectonic stress fields in Israel

A majority of the joints observed in Nahal Neqarot trend NNW or WNW, suggesting that they propagated in the presence of the DSS and SAS, respectively. The different timing relations derived from fracture intersections for the two sets at different stations, and among different beds at the same station, is strong evidence in support of the proposed fluctuating stress field model of Eyal (1996). Dunne and North (1990) reported mutually cross-cutting relations for two sets of orthogonal veins in southwestern Wales. They proposed that fracturing occurred in response to a uniformly oriented orogenic compression, and that intermediate and least principal stresses differed only slightly in magnitude. As a result of the alternating intermediate and least principal stresses, opening-mode fractures formed at 90° to each other, resulting in the observed cross-cutting relations. Bahat (1988) also observed alternating abutting relations for two orthogonal, bed-confined joint sets in Eocene chalks near Beer-Sheva, Israel. At Nahal Neqarot, however, the DSS and SAS joint trends are not orthogonal but differ by 52°. Therefore, their formation cannot be attributed to stress relaxation within a single regional stress field in which σ_2 and σ_3 switch positions, but rather is a reflection of two distinct and superimposed regional stress fields.

Our schematic model for neotectonic stress fields in southern Israel since the Miocene incorporates two main results from the Neqarot study. First, the WNW joints are mostly absent from the less competent marly limestone and chalky limestone beds, implying that these lithologies did not fracture in the presence of the SAS (Fig. 13). This behavior resulted in a mechanical stratigraphy consisting of SAS joints in the competent limestone beds and the absence of SAS joints in the less competent beds. On the other hand, DSS-compatible joints are found in all studied competent lithologies (limestones, chalky limestones, marly limestones). Second, the higher FSR for the NNW joint set implies that the S_H-normal extensional strain associated with the DSS is greater than the S_H-normal extensional strain resulting from the SAS. As noted earlier, the collection of joint spacing data in this study specifically avoided zones of localized strain adjacent to fault and fracture zones; therefore, the high FSRs for the NNW set reflect a more regional rather than local strain. Furthermore, because many beds exceed by far the proposed "saturation" level of FSI = 1.5 for NNW joints, we conclude that the magnitude of extensional strain associated with the DSS is relatively high, certainly much higher than the strain related to the SAS.

The DSS is related to displacement along the Dead Sea transform and structures compatible with this stress field are found up to 200–250 km on either side of this plate boundary. On the other hand, the plate-scale SAS influences a much larger area (i.e. the entire African plate). We envision a stress field in Nahal Neqarot (located about 50–60 km from the DST) that is comprised of a more dominant but episodic DSS superimposed on a background SAS of lesser intensity. A large-magnitude earthquake in the vicinity of the DST will release the cumulative stress derived from various sources, mainly the DSS and SAS. The DSS fluctuates through time, whereas the SAS may be rather constant. We suggest that the greater intensity of the DSS causes stress to gradually build along major regional faults associated with the DST (Fig. 13). Joints that develop during this stage are aligned parallel to S_H of the DSS (340–160°), display higher FSRs, and occur in

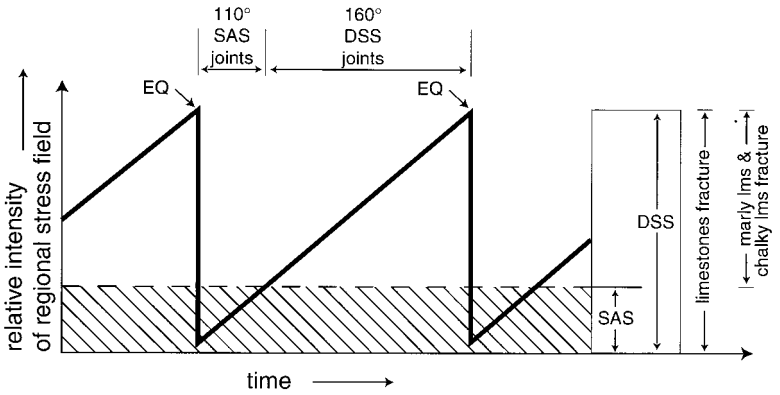

Fig. 13. Schematic representation of the formation of SAS- and DSS-compatible joints with respect to the model proposed by Eyal (1996) of superimposed and fluctuating regional stress fields since the middle Miocene. The DSS is the more dominant stress regime, and joints develop in all lithologies during interseismic periods. Immediately after major earthquakes (EQ), the stress related to the DSS drops dramatically and the remote SAS controls joint orientation. However, SAS-compatible joints only develop in the limestones because the intensity of the SAS is not large enough to fracture marly limestone and chalky limestone beds.

marly limestone, chalky limestone, and limestone beds. Eventually, a major earthquake occurs along a segment of the DST, resulting in a large stress drop and the temporary dominance of the SAS. This temporary replacement of the DSS by the SAS may be restricted only to regions adjacent to the DST, such as Nahal Neqarot, and not to the entire African plate. Joints that propagate during this period are aligned parallel to the SAS (290–110°), have lower FSRs, and mostly occur only in limestones (Fig. 13).

7. Conclusions

The two most prominent joint sets observed in carbonate beds of the Gerofit formation in Nahal Neqarot are aligned NNW and WNW, and are compatible with the DSS and SAS, respectively. Cross-cutting relations of these joint sets and the other less prominent joint sets reveal different timing relationships. In some beds, the WNW set consistently predates the NNW set, whereas in other beds the NNW set predates the WNW set. These results support the Eyal (1996) model of two major stress field regimes in Israel that fluctuated through time since the middle Miocene. The joint data suggest abrupt changes rather than gradual rotations in stress field orientations.

Extensional strain normal to S_H associated with the DSS is greater than that of the SAS because (a) lithologies that remain unfractured during periods of SAS are jointed in response to the DSS, and (b) the FSRs are much greater for joints belonging to the DSS. Finally, trends of joints and other opening-mode fractures have been used to map regional stress fields, both past and present. Specifically, joint trends were used to determine the *orientations* of maximum and minimum horizontal stresses, and to construct trajectories of regional stress fields. In this study we propose that the FSR can serve as an effective tool to estimate the relative *magnitudes* of regional stress fields, because the FSR may be considered a proxy for strain.

Acknowledgements

Many of the structural relations and concepts discussed in this paper were the focus of Paul Hancock's broad research interests in brittle microtectonics (Hancock, 1969, 1985; Hancock et al., 1984; Bevan and Hancock, 1986; Dunne and Hancock, 1994) and neotectonics (Hancock and Barka, 1987; Hancock, 1988; Hancock and Engelder, 1989; Stewart and Hancock, 1990, 1991; Hancock, 1991). Our research has greatly benefited from Paul Hancock's contributions in these fields, and we are honored to contribute to the special issue of the *Journal of Structural Geology* celebrating Paul's accomplishments. Funding for this research was provided by the United States–Israel Binational Science Foundation Grant 94-00396. We benefited from discussions with Martin Finn, Juan-Carlos Ortiz, and Scott Wilkins. Excellent reviews by Paul Gillespie, Roy Gabrielsen, and William Dunne greatly improved the paper.

References

Baer, G., Reches, Z., 1989. Doming mechanisms and structural development of two domes in Ramon, southern Israel. Tectonophysics 166, 293–315.

Bahat, D., 1986. Joints and en echelon cracks in Middle Eocene chalks near Beer Sheva, Israel. Journal of Structural Geology 8, 181–190.

Bahat, D., 1987. Jointing and fracture interactions in middle Eocene chalks near Beer-Sheva, Israel. Tectonophysics 136, 299–321.

Bahat, D., 1988. Early single-layer and late multi-layer joints in the Lower Eocene chalks near Beer Sheva, Israel. Annales Tectonicae 2, 3–11.

Bahat, D., 1999. Single-layer burial joints vs single-layer uplift joints in Eocene chalk from the Beer Sheva syncline in Israel. Journal of Structural Geology 21, 293–303.

Bai, T., Pollard, D.D., 2000. Fracture spacing in layered rocks: a new explanation based on the stress transition. Journal of Structural Geology 22, 43–57.

Bartov, J., 1974. A structural and paleogeographic study of the central Sinai faults and domes. Ph.D. thesis, Hebrew University of Jerusalem.

Bartov, Y., Steinitz, G., Eyal, M., Eyal, Y., 1980. Sinistral movement along

the Gulf of Aqaba—its age and relation to the opening of the Red Sea. Nature 285, 220–222.
Becker, A., 1994. Bedding-plane slip over a pre-existing fault, an example: the Ramon Fault, Israel. Tectonophysics 257, 223–237.
Becker, A., Gross, M.R., 1996. Mechanism for joint saturation in mechanically layered rocks: an example from southern Israel. Tectonophysics 257, 223–237.
Ben-David, R., 1992. The geology of Be'erot Oded area and western Makhtesh Ramon, and stages in the evolution of landscape since the late Miocene to the Present. M.Sc. thesis, Ben-Gurion University.
Bentor, Y.K., Vroman, A., 1954. A structural contour map of Israel 1:250,000, with remarks on the dynamic interpretation. Geological Survey of Israel Bulletin 7.
Bentor, Y.K., Vroman, A., 1960. The Geological Map of Israel Sheet 16: Mount Sedom, 2nd edn. Geological Survey of Israel scale: 1:100,000.
Bevan, T.G., Hancock, P.L., 1986. A late Cenozoic regional mesofracture system in southern England and northern France. Journal of the Geological Society of London 143, 355–362.
Bogdonov, A.A., 1947. The intensity of cleavage as related to the thickness of beds. Soviet Geology 16, 000 in Russian.
Dunne, W.M., Hancock, P.L., 1994. Palaeostress analysis of small-scale brittle structures. In: Hancock, P.L. (Ed.), Continental Deformation, Pergamon Press, Oxford, pp. 101–120.
Dunne, W.M., North, C.P., 1990. Orthogonal fracture systems at the limits of thrusting: an example from southwestern Wales. Journal of Structural Geology 12, 207–215.
Dyer, R., 1988. Using joint interactions to estimate paleostress ratios. Journal of Structural Geology 10, 685–699.
Eidelman, A., Reches, Z., 1992. Fractured pebbles—a new stress indicator. Geology 20, 307–310.
Engelder, T., 1982. Is there a genetic relationship between selected regional joints and contemporary stress within the lithosphere of North America? Tectonics 1, 161–177.
Engelder, T., 1985. Loading paths to joint propagation during a tectonic cycle: an example from the Appalachian Plateau, U.S.A. Journal of Structural Geology 7, 459–476.
Engelder, T., Geiser, P.A., 1980. On the use of regional joint sets as trajectories of paleostress fields during the development of the Appalachian Plateau, New York. Journal of Geophysical Research 85, 6319–6341.
Engelder, T., Gross, M.R., Pinkerton, P., 1997. Joint development in clastic rocks of the Elk Basin anticline, Montana–Wyoming: an analysis of fracture spacing versus bed thickness in a basement-involved Laramide structure. In: Hoak, T.E., Klawitter, A.L., Blomquist, P.K. (Eds.), Fractured Reservoirs; Characterization and Modeling, Rocky Mountain Association of Geologists, pp. 1–18.
Eyal, M., Eyal, Y., Bartov, Y., Steinitz, G., 1981. The tectonic development of the western margin of the Gulf of Elat (Aqaba) Rift. Tectonophysics 80, 39–66.
Eyal, Y., 1996. Stress field fluctuations along the Dead Sea Rift since the middle Miocene. Tectonics 15, 157–170.
Eyal, Y., Reches, Z., 1983. Tectonic analysis of the Dead Sea rift region since the Late Cretaceous based on mesostructures. Tectonics 2, 167–185.
Fischer, M.P., 1994. Application of linear elastic fracture mechanics to some problems of fracture propagation in rock and ice. Ph.D. thesis, Pennsylvania State University.
Fischer, M.P., Gross, M.R., Engelder, T., Greenfield, R.J., 1995. Finite element analysis of the stress distribution around a pressurized crack in layered elastic medium: implications for the spacing of natural hydraulic fractures in bedded sedimentary rock. Tectonophysics 247, 49–64.
Garfunkel, Z., 1964. Tectonic problems along the Ramon lineament. M.Sc. Thesis, Hebrew University of Jerusalem.
Garfunkel, Z., 1981. Internal structure of the Dead Sea leaky transform (Rift) in relation to plate kinematics. Tectonophysics 80, 81–108.
Garfunkel, Z., Bartov, Y., 1977. The tectonics of the Suez Rift. Israel Geological Survey Bulletin 71, 44 p.
Garrett, K.W., Bailey, J.E., 1977. Multiple transverse fracture in 90° cross-ply laminates of a glass fibre-reinforced polyester. Journal of Materials Science 12, 157–168.
Gillespie, P.A., Howard, C.B., Walsh, J.J., Watterson, J., 1993. Measurement and characterization of spatial distributions of fractures. Tectonophysics 226, 113–141.
Gillespie, P.A., Johnston, J.D., Loriga, M.A., McCaffrey, K.J.W., Walsh, J.J., Watterson, J., 1999. Influence of layering on vein systematics in line samples. In: McCaffrey, K.J.W., Lonergan, L., Wilkinson, J.J. (Eds.), Fractures, Fluid Flow and Mineralization. Geological Society Special Publication 155. Geological Society, pp. 35–56.
Gross, M.R., 1993. The origin and spacing of cross-joints: examples from the Monterey Formation, Santa Barbara coastline, California. Journal of Structural Geology 15, 737–751.
Gross, M.R., Engelder, T., 1991. A case for neotectonic joints along the Niagara Escarpment. Tectonics 10, 631–641.
Gross, M.R., Engelder, T., 1995. Strain accommodated by brittle failure in adjacent units of the Monterey Formation, U.S.A.: scale effects and evidence for uniform displacement boundary conditions. Journal of Structural Geology 17, 1303–1318.
Gross, M.R., Fischer, M.P., Engelder, T., Greenfield, R.J., 1995. Factors controlling joint spacing in interbedded sedimentary rocks: integrating numerical models with field observations from the Monterey Formation, USA. In: Ameen, M.S. (Ed.), Fractography: Fracture Topography as a Tool in Fracture Mechanics and Stress Analysis. Geological Society Special Publication 92, Geological Society, pp. 215–233.
Gross, M.R., Bahat, D., Becker, A., 1997. Relations between jointing and faulting based on fracture-spacing ratios and fault-slip profiles: a new method to estimate strain in layered rocks. Geology 25, 887–890.
Hancock, P.L., 1969. Fracture patterns in the Cotswold Hills. Proceedings of the Geological Association 80, 219–241.
Hancock, P.L., 1985. Brittle microtectonics: principles and practice. Journal of Structural Geology 7, 437–457.
Hancock, P.L., 1988. Neotectonic fractures formed during extension at shallow crustal depths. Memoir of the Geological Society of China 9, 201–226.
Hancock, P.L., 1991. Determining contemporary stress directions from neotectonic joint systems. Philosophical Transactions of the Royal Society of London A337, 29–40.
Hancock, P.L., AlKadhi, A., Sha'at, N.A., 1984. Regional joint sets in the Arabian platform as indicators of intraplate processes. Tectonics 3, 27–43.
Hancock, P.L., Barka, A.A., 1987. Kinematic indicators on active normal faults in western Turkey. Journal of Structural Geology 9, 573–584.
Hancock, P.L., Engelder, T., 1989. Neotectonic joints. Geological Society of America Bulletin 101, 1197–1208.
Hobbs, D.W., 1967. The formation of tension joints in sedimentary rocks: an explanation. Geological Magazine 104, 550–556.
Holst, T.B., Foote, G.R., 1981. Joint orientation in Devonian rocks in the northern portion of the lower peninsula of Michigan. Geological Society of America Bulletin 92, 85–93.
Huang, Q., Angelier, J., 1989. Fracture spacing and its relation to bed thickness. Geological Magazine 126, 355–362.
Ji, S., Saruwatari, K., 1998. A revised model for the relationship between joint spacing and layer thickness. Journal of Structural Geology 20, 1495–1508.
Ji, S., Zhu, Z., Wang, Z, 1998. Relationship between joint spacing and bed thickness in sedimentary rocks; effects of interbed slip. Geological Magazine 135, 637–655.
Joffe, S., Garfunkel, Z., 1987. Plate kinematics of the circum Red Sea—a re-evaluation. Tectonophysics 141, 5–22.
Krenkel, E., 1924. Der Syrische Bogen. Zentarbladt fur Mineralogie, Geologie, Palaeontologie 9, 301–313 10, 274–281.
Lachenbruch, A.H., 1961. Depth and spacing of tension cracks. Journal of Geophysical Research 66, 4273–4292.
Ladeira, F.L., Price, N.J., 1981. Relationship between fracture spacing and bed thickness. Journal of Structural Geology 3, 179–183.

Letouzey, J., Tremolieres, P., 1980. Paleo-stress fields around the Mediterranean derived from microtectonics: comparison with plate tectonic data. Rock Mechanics 9, 173–192.

Muller, O.H., Pollard, D.D., 1977. The stress state near Spanish Peaks, Colorado, determined from a dike pattern. Pure and Applied Geophysics 115, 69–86.

Narr, W., Suppe, J., 1991. Joint spacing in sedimentary rocks. Journal of Structural Geology 13, 1037–1048.

Pollard, D.D., Aydin, A., 1988. Progress in understanding jointing over the past century. Geological Society of America Bulletin 100, 1181–1204.

Price, N.J., 1966. Fault and Joint Development in Brittle and Semi-Brittle Rocks. Pergamon Press, Oxford.

Rabinovitch, A., Bahat, D., 1999. Model of joint spacing distribution based on shadow compliance. Journal of Geophysical Research 104, 4877–4886.

Rawnsley, K.D., Rives, T., Petit, J.-P., Hencher, S.R., Lumsden, A.C., 1992. Joint development in perturbed stress fields near faults. Journal of Structural Geology 14, 939–951.

Renshaw, C.E., 1997. Mechanical controls on the spatial density of opening-mode fracture networks. Geology 25, 923–926.

Rives, T., Razack, M., Petit, J.-P., Rawnsley, K.D., 1992. Joint spacing: analogue and numerical simulations. Journal of Structural Geology 14, 925–937.

Ruf, J.C., Rust, K.A., Engelder, T., 1998. Investigating the effect of mechanical discontinuities on joint spacing. Tectonophysics 295, 245–257.

Sbar, M.L., Sykes, L.R., 1973. Contemporary compressive stress and seismicity in eastern North America: an example of intra-plate tectonics. Geological Society of America Bulletin 84, 1861–1882.

Selverstone, J., 1988. Evidence for east–west crustal extension in the eastern Alps: implications for the unroofing history of the Tauren Window. Tectonics 7, 87–105.

Srivastava, D.C., Engelder, T., 1990. Crack-propagation sequence and pore-fluid conditions during fault-bend folding in the Appalachian Valley and Ridge, central Pennsylvania. Geological Society of America Bulletin 102, 116–128.

Stewart, I.S., Hancock, P.L., 1990. Brecciation and fracturing within neotectonic normal fault zones in the Aegean region. In: Knipe, R.J., Rutter, E.H. (Eds.), Deformation Mechanisms, Rheology and Tectonics. Geological Society of London Special Publication 54, Geological Society, London, pp. 105–119.

Stewart, I.S., Hancock, P.L., 1991. Scales of structural heterogeneity within neotectonic normal fault zones in the Aegean region. Journal of Structural Geology 13, 191–204.

Tapponnier, P., Peltzer, G., Le Dain, A.Y., Armijo, R., Cobbold, P., 1982. Propagating extrusion tectonics in Asia: new insights from simple experiments with plasticine. Geology 10, 611–616.

Wu, H., Pollard, D.D., 1995. An experimental study of the relationship between joint spacing and layer thickness. Journal of Structural Geology 17, 887–905.

Zoback, M.L., 1992. First- and second-order patterns of stress in the lithosphere: the world stress project. Journal of Geophysical Research 97, 11,703–11,728.

Zoback, M.L., Zoback, M.D., 1980. State of stress in the conterminous United States. Journal of Geophysical Research 85, 6113–6156.

Zoback, M.L., Zoback, M.D., 1989. Tectonic stress field of the continental United States. In: Pakiser, L.C., Mooney, W.D. (Eds.), Geophysical Framework of the Continental United States. Geological Society of America Memoir 172, Geological Society of America, pp. 523–539.